Journal of Power Sources 182 (2008) 76–82

Contents lists available at ScienceDirect

Journal of Power Sources

journal homepage: www.elsevier.com/locate/jpowsour

Magnetic resonance imaging investigation of water accumulation and transport in graphite flow fields in a polymer electrolyte membrane fuel cell: Do defects control transport?

Zachary W. Dunbar, Richard I. Masel*

Department of Chemical and Biomolecular Engineering, University of Illinois, 600 S Mathews, Urbana, IL 61801, United States

ARTICLE INFO

Article history:
Received 23 January 2008
Accepted 18 March 2008
Available online 29 March 2008

Keywords:
Magnetic resonance imaging
PEM fuel cell
Water management
Hydrogen economy
Nafion membrane
Wavy-stratified flow

ABSTRACT

Water management remains a leading challenge in the implementation of polymer electrolyte membrane (PEM) fuel cells. At present there are many excellent models for the distribution of water within PEM fuel cells, but little quantitative data on the water distribution that can be compared to models. In this paper magnetic resonance imaging (MRI) is used to examine and quantify the flow of water in graphite coated flow fields in a miniature PEM (hydrogen) fuel cell. It was found as with Teflon® flow fields, that the water accumulated in waves along the bottom of the flow field. The water waves moved very slowly through the flow channels and seem to get stuck on tiny defects in the flow field. The water accumulated at the defect, until the wave nearly bridged the gap between the cathode and the bottom of the flow field. Then the water wave was pushed along to the next defect. Surprisingly, the current out of the cell was nearly constant as waves accumulated and were swept away, even though the flow was clearly not at steady state. These results show that small defects in the wall of the flow field play a critical role in water transport in the flow fields.

1. Introduction

Water management is still a major challenge in polymer electrolyte membrane (PEM) fuel cells. There are many excellent models of the water distribution as reviewed by Cheddie and Monroe [1], Ma et al. [2] and Wang [3]. According to Ma et al. [2], however, the progress on modeling has been limited by a lack of quantitative data. Neutron scattering has provided two-dimensional pictures of the water in fuel cells [4–9], but extensions to three dimensions, and quantification of the spacial data has been difficult. Magnetic resonance imaging (MRI) has often been used to examine water motion within a proton conducting membrane [10–29] and a few studies using MRI have been done to examine water in the membranes of operating fuel cells [29–35]. However, data for spatial distributions of water in the flow fields in a quantitative way remain scarce.

In a previous paper [36] we used MRI imaging to examine water transport in Teflon® flow fields in a miniature PEM fuel cell. We found that water flow was not as expected from previous models. The water did not form slugs which are rapidly transported down the flow field. Instead, the water accumulates in waves along the bottom of the flow field (i.e. away from the MEA). The waves slowly move through the flow channel, as expected for wavy-stratified flow.

In this paper, we extend the measurements to examine water flow in graphite coated flow fields. We find that waves still form as was described in our previous paper. In a perfect flow field, the waves move slowly along the bottom of the flow field, but in our actual flow fields the water waves appear to get stuck at surface defects in the flow channel. After sufficient water build up, the waves will 'slip' further down the flow channel, before becoming stuck again on a defect further along the flow channel. The results are qualitatively different than anything that has been observed previously, but easily understood theoretically.

2. Experimental design

The experiments were done in the miniature MRI compatible fuel cell described in our previous work [36] (see Fig. 1). The fuel cell was comprised of Teflon® flow fields, solid gold current collectors and carbon cloth gas diffusion layers (GDLs), Teflon® treated on the cathode side. The MEA membrane was Nafion 115 (Ion Power) and both the anode and cathode catalyst were 40% platinum on carbon (Tanaka). The catalysts were applied with the direct paint technique

* Corresponding author. Tel.: +1 217 333 6841; fax: +1 217 333 5052.
E-mail address: r-masel@uiuc.edu (R.I. Masel).

0378-7753/$ – see front matter © 2008 Elsevier B.V. All rights reserved.
doi:10.1016/j.jpowsour.2008.03.057

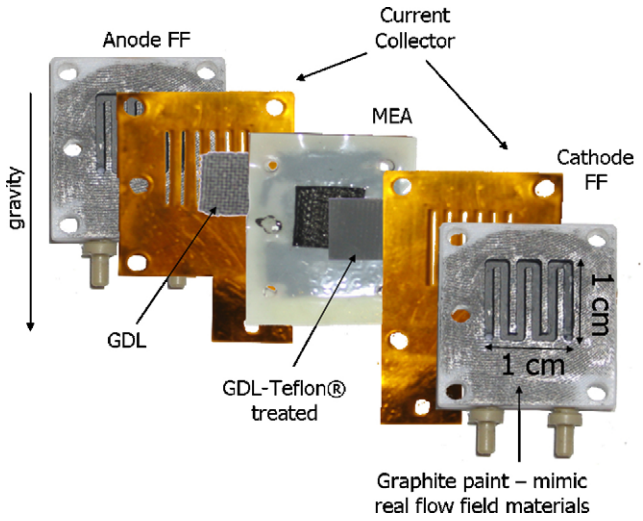

Fig. 1. A photograph of the fuel cell used in the study. The flow fields are comprised of Teflon®, with a thin graphite coating painted onto the actual flow channels to simulate the hydrophobicity of a commercial solid graphite flow field. The current collectors are machined from thin pieces of solid gold. The gas diffusion layers are carbon cloth (E-Tek), Teflon® treated for the cathode side. The MEA is composed of Pt on carbon from Tanaka, 4 mg cm^{-2}, on both the anode and cathode. The membrane used was Nafion 115 (Ion Power).

[37]. The fuel cell was oriented vertically in the MRI (Fig. 2) and had a total active area of 1 cm^2 on each electrode.

It is important to note the necessity of constructing the fuel cell out of materials that are compatible with the strong magnetic field present inside the MRI machine. Ferromagnetic materials are completely unsuitable (anything containing iron, nickel or cobalt). Any material with high conductivity (graphite, gold and copper) must only be used in small quantities. This is due to induced electrical eddy currents in the conductive object, caused by the MRI gradient magnets. These currents obscure the signal from water, and increase the noise of the overall signal.

A unique feature of the flow fields of this fuel cell was that they were painted with a graphite layer (Aquadag), to more accurate mimic the hydrophobicity of a commercially available pure graphite flow field, instead of the extremely hydrophobic Teflon® material from which the flow fields were machined. Pure graphite flow fields would be incompatible with the strong magnetic field in the MRI machine. The flow channels were 1 mm in width, and 3 mm in depth. The flow channels were machined in a serpentine pattern, as is visible in Fig. 1.

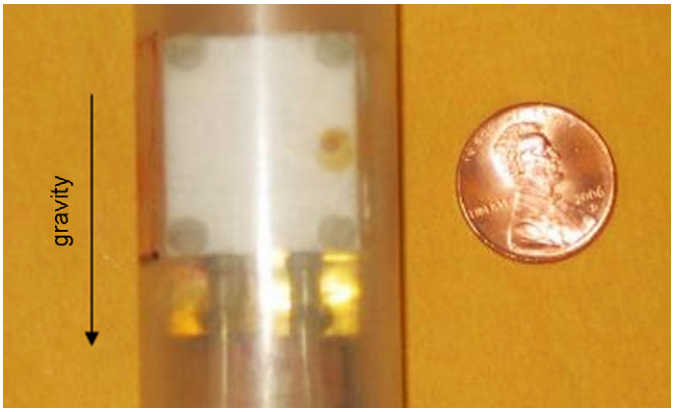

Fig. 2. The assembled MRI compatible fuel cell. The fuel cell is placed in a fitted holder, in order to ensure proper alignment inside the MRI. The gravity vector is shown, to indicate fuel cell orientation.

Humidified hydrogen gas was supplied to the anode flow field, at the rate of 10 sccm. Humidified oxygen gas was supplied to the cathode, also at 10 sccm. This resulted in a linear gas velocity in the flow channels of approximately 5.5 cm s^{-1}. Twisted pair wire was used to withdraw current from the fuel cell. An electronic load (Agilent 6060B) was used to maintain the fuel cell at a constant current of 500 mA cm^{-2}. Voltage was measured and recorded using a digital logging multimeter (Fluka 189).

As described previously [36], water filled capillaries (internal diameter 0.5 mm) were attached to the fuel cell, in order to provide a calibration standard for MRI imaging of the interior of the fuel cell.

2.1. MRI operation and data reconstruction

The fuel cell was placed vertically inside the imaging scanner as shown in Fig. 2. The scanner was an Oxford Instruments, Abington, UK magnet equipped with a Unity/Inova console (Varian, Palo Alto, CA), operating at 14.1 T with a bore of an internal diameter of 5 cm. Varian transmitter/receiver quadrature RF coil was used with an internal diameter of 3.0 cm. T2-weighted coronal (along a vertical axis) two-dimensional sections were acquired using a Spin-Echo multi slice pulse sequence.

The images were acquired slice by slice, with a 0.5 mm gap. The acquisition time for each sequence was 4 min and 19 s. The repetition time was 1000 ms, and echo time 10 ms. Two transients/averages were taken. The spectral width was 71 kHz, and the field of view was 5.0 cm × 2.5 cm. Each voxel represented a volume 138 μm high × 138 μm wide × 200 μm thick. Water intensity signal was recorded for each voxel. The data was stored to a data file that was analyzed using MATLAB software.

A MATLAB program written in house reconstructed the MRI data to a bitmap image. Additionally, the program utilized data gathered from the reference capillaries to calibrate the signal generated from the MRI with the signal generated by pure water. In this manner, the signal data generated by the MRI could be converted to water concentration data [36].

As a final step to aid the understanding by the reader, the MRI data was superimposed over a digital image of the fuel cell flow field. This enables the reader to clearly envision exactly where the water is located spatial in the fuel cell. On many of these images, a cartoon image of a gas diffusion layer was added, to aid in understanding how the water is distributed with respect to the fuel cell and its constituent components.

3. Results

3.1. Initial water formation

Fig. 3 shows a MRI image of one of the low channels in the fuel cell soon after the fuel cell started drawing current. To orient the reader this image was made by superimposing the MRI image and a photograph of the fuel cell. The blue dotted line near the center of the cell overlays the position of the Nafion membrane. The gray box overlays the position of the carbon cloth. The line of blue dots along the right side of the picture is the position of the bottom of the cathode flow field. The red region represents a 2 mm diameter water drop. There is no water seen in the carbon cloth due to an imaging artifact: the carbon paper blocks the MRI image. After applying a load to the cell, water begins to form in the cathode catalyst layer. Some of the water moves into the Nafion® membrane, while some of it enters the cathode gas diffusion layer, eventually

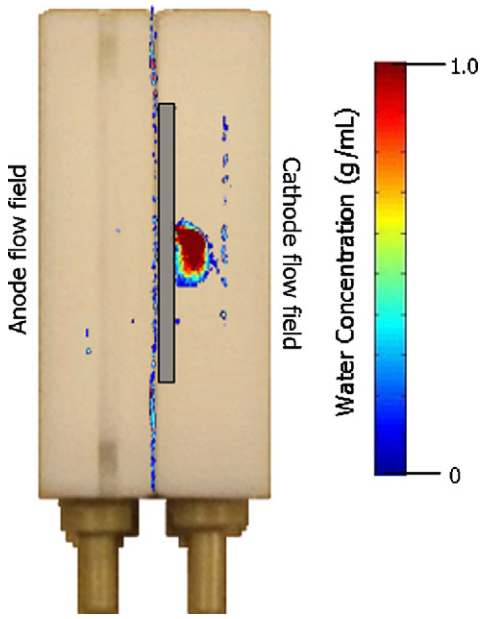

Fig. 3. An MRI image taken soon after the fuel cell started drawing current. Humidified hydrogen at 10 sccm and humidified air at 10 sccm are supplied to the anode and cathode, respectively. The cell is placed under a load of 500 mA cm^{-2}. To orient the reader this image was made by superimposing the MRI image and a photograph of the fuel cell. The blue dotted line near the center of the cell overlays the position of the Nafion membrane. The gray box overlays the position of the carbon cloth. The line of blue dots along the right side of the picture is the position of the bottom of the flow field. The red region is a small water drop sitting on top of the carbon cloth. There is no water seen in the carbon cloth due to an imaging artifact: the carbon paper blocks the MRI image. This figure shows that initially water accumulates in drops on the cathode flow field. (For interpretation of the references to color in this figure legend, the reader is referred to the web version of the article.)

migrating through the porous GDL, and 'breaking through' on the GDL surface. Initially, only large droplets of water were present, clinging to the Teflon® treated GDL. There was no water detectable in the anode region of the fuel cell.

3.2. Approach to steady state

After about 15 min of operation, running at 500 mA cm^{-2} with humidified gas streams, the situation changes entirely. Large water drops are no longer seen on the GDL. Instead, there are tiny water drops on the top of the carbon paper and large water waves sitting along the bottom of the flow fields as illustrated in Fig. 4. Initially, the waves slowly move down the flow channel, but after a few minutes the waves seem to get stuck. Afterward the waves continue to grow by accumulation of water, but the waves are largely stationary within the flow field.

During the rest of the measurements the MRI images look the same. We occasionally could observe evidence for slow movement of a water wave, but many of the waves got stuck at various places in the flow field.

Interestingly, higher resolution images reveal that there is always a gap between the water wave and the GDL. Air flows through the gap so we can maintain a high air flow rate even though the water wave is stationary.

Chronoamperometry reveals that the current is nearly constant as water accumulates even though the flow channel is nearly flooded. Thus, even though the water accumulation has almost filled the flow channels, the water has no affect on the fuel cell performance. However, in a fuel cell operated under 'real world' temperature conditions, it would affect the freeze resistance.

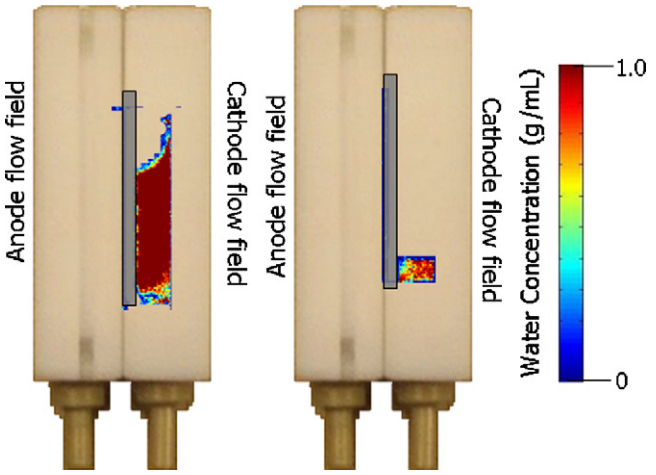

Fig. 5. An MRI image (left) of a nearly filled channel just before the fluid wave slips, and (right) an image of the same channel 12 min later. Air flows from the top to the bottom in the figure. You cannot see it in the image, but there is a gap between the water wave and the Teflon(R) treated gas diffusion layer.

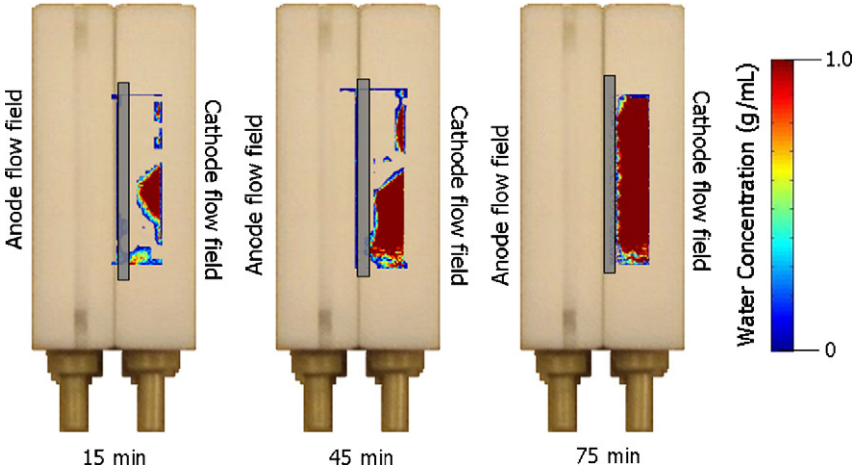

Fig. 4. A picture of some of the waves that form in the flow channels. Humidified hydrogen at 10 sccm and humidified air at 10 sccm are supplied to the anode and cathode, respectively. Notice that in each case the wave sits along the bottom of the flow channel. It is not obvious from the picture, but higher resolution images show that the water wave does not touch the membrane. Instead a small gap remains between the GDL and the water, allowing air to blow around the water wave.

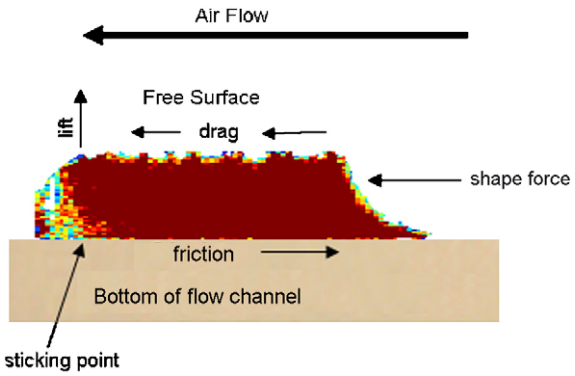

Fig. 6. A diagram of the forces on the water wave just before it slips. The moving air creates a shape (drag) force pushing along the front surface, and a viscous drag force because of the air blowing across the top surface. Friction from the bottom wall slows the motion down. There is also a lift force near the front edge that produces the Jeffries waves.

3.3. Water accumulation and method of movement

Of course, the water has to be eventually transported out of the cell, or else the reaction on the cathode will stop. Figs. 5–7 illustrate the mechanism of water motion. The image on the left of Fig. 5 shows a channel that is nearly completely filled. There is still a gap along the top of the flow channel, but the shape of the wave is different than in the earlier pictures. First we can observe what appear to be small Jeffries waves (i.e. nearly periodic waves like those in the ocean) on the top of the larger wave. Then there is significant curvature on the upper and lower surfaces of the water wave. Notice that something is pushing the water wave forward.

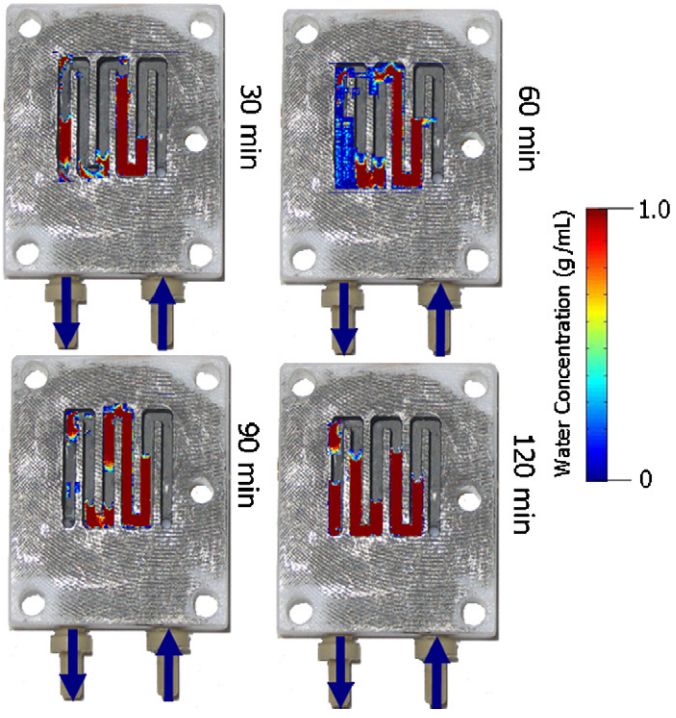

Fig. 7. A top view of the cathode flow field illustrating the position of the water waves. The arrows indicate the direction of gas flow. The waves are stationary most of the time but periodically, a wave will 'slip' from one location in the flow channel to another. The blue trail in the 60 min scan is associated with a wave that slipped. One can estimate the slip velocity from the length and color of the tail. From this we estimate a slip velocity of in the order of 0.04 cm s^{-1} compared to an air velocity of 5.5 cm s^{-1}. (For interpretation of the references to color in this figure legend, the reader is referred to the web version of the article.)

Fig. 6 illustrates the forces on the water wave in Fig. 5. The air exerts two different forces on the wave, a shape (drag) force that pushes the wave along, and a viscous drag force along the top surface of the wave. The two forces push the wave forward. The combination of the shape force and the viscous force on the top surface of the water wave causes the free surface of the water wave to move in the direction of the air flow.

Note also, that if there was no free surface, one would not see this effect. Instead, the wave would assume a parabolic shape due to the no slip condition on the surface touching the GDL.

The water wave was essentially stable when we were taking the left image in Fig. 5 but, the water wave started to move soon after we took the image in Fig. 5. We did not take intermediate images, but after we finished, we found that when the next image was taken 12 min later, the water wave disappeared from the flow channel.

Fig. 7 shows some top images during fuel cell operation. If we start with the image taken starting 30 min after the fuel cell began operation, we see water in a few of the channels, and no obvious fluid motion. This image makes it seem as though the flow channel is filled, but images taken perpendicular to the flow direction show that there is actually a gap between the top of the water wave and the GDL. At 60 min, the picture looks somewhat different. In addition to the water filled channels, there are light blue regions, where the channel is not filled.

The light blue regions are indicative of water motion. The scans in Fig. 7 were taken slowly so we could get high enough resolution to image the gaps between the water wave and the GDL and the Jeffries waves above the larger water wave. The image, then, is a 259 s average of the water position. If the water is stationary, it would appear as a red section in the image, but if the water is moving, the water is only in the image for part of the time, so the water appears blue.

One can get an idea of the water velocity from the color. The blue color corresponds to the water being in the image about 10% of the time. If we assume that the water wave was in the image for 10% of the 259 s, and traveled about 1 cm during that time, then the average water velocity comes out to be 1 cm/25.9 s $\cong$ 0.04 cm s^{-1}. This compares to an average air velocity of 5.5 cm s^{-1}. Of course, from a single observation one cannot tell if the wave was moving slowly, or was quickly transported out of the flow channel after 10% of the time elapsed. However, we have many observations and always observe the same light blue color whenever a water wave exhibits movement inside the flow field. Therefore we conclude that when the water wave moves, its velocity is much slower than the velocity of the air.

The implication of Figs.5 and 7 is that the water motion follows a 'slip and stick' mode of transport. The water waves are stationary most of the time, but every so often one of the water waves gets unstuck. The wave then moves down the channel until it gets stuck again.

3.4. Location of standing waves and flow field defects

Fig. 7 also shows another interesting phenomenon. Notice that the water waves seem to always get stuck at the same locations. After approximately 30 min of operation, there were multiple location in the flow channels were water waves were present. It seemed odd that despite taking images many minutes apart, the waves always seemed to appear in approximately the same locations. It was theorized that perhaps the waves were becoming 'stuck' in the flow channels at certain points, perhaps due to defects or non-uniformities in the surface of the flow channel.

We tried carefully examining the flow channel to see if we could find defects that would account for the sticking. We could not see

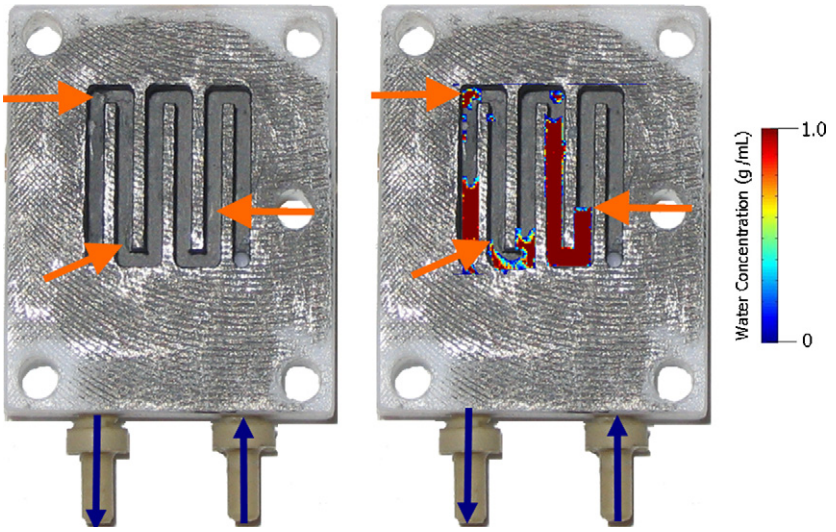

Fig. 8. A high contrast picture of the flow fields. Notice that there are visible defects at the places where the water gets stuck.

any defects with our naked eyes, but when we took photographs of the flow channels, and increased the contrast we were able to see defects that could account for the sticking process. Fig. 8 shows a high contrast image of the flow channel and there are certainly non-uniformities present in the graphite coating of the flow channels. Three of these defects and the location of 'stuck' water waves are shown. Clearly, the slip and stick phenomenon we observe could be explained by these defects although, that is not completely clear.

3.5. Electroosmosis vs. diffusion

A final observation was made regarding the effect of current density on water distribution in the anode flow fields. Although water is generated at the cathode, it is possible for water to enter the anode flow field by passing through the water permeable Nafion® membrane. There are two driving forces for this movement of water across the membrane. There is a water concentration gradient from the high water content cathode to the low water content anode. This induces a diffusive force. The second force is a hydrophobic backpressure force exerted by the Teflon® treated carbon cloth GDL, which is sandwiched on top of the cathode catalyst layer.

There is also an electroosmotic force working in opposition to both diffusion and the hydrophobic back pressure. The electroosmotic force is cause by the diffusion of protons from the anode catalyst to the cathode catalyst. These protons 'drag' water with them during the migration, potentially dehydrating the anode.

When running at high currents, there was no water detectable in the anode flow field. Conversely, at low currents, there was water visible in the anode flow field, correlating to a location directly across the membrane from the area of highest water concentration on the cathode. Thus it appears that at 200 mA cm^{-2}, the rate of diffusion of water back through the membrane is larger than the rate of water transport due to electroosmotic drag, while the opposite occurs at 500 mA cm^{-2} or higher.

4. Discussion

Many of the experimental results were as expected, but there were also some surprises. The key surprise here was the 'stick and slip' mode of fluid transport. Most previous investigators had assumed that the water is moving in slugs down the flow channel. The two-phase flow literature indicates that one usually does not observe slug flow unless the volumetric flow rate of the liquid water is comparable to the volumetric flow rate of the air [38–40] which is not the case in a fuel cell. Still, slug flow has been widely assumed.

We have never observed slug flow. In slug flow, the water should move at the same velocity as the gas. We have never seen any evidence of fast moving water. Instead, the water generated at the cathode transports deep into the cathode flow fields, where it accumulates and only moves slowly through the flow field. We estimate a water velocity of in the order of 0.04 cm s^{-1} compared to an air velocity of 5.5 cm s^{-1}. Clearly, the water is not moving at the air velocity so we do not have slug flow.

The closest analogy from the two-phase flow literature is wavy-stratified flow as was discussed in our previous paper [36]. In wavy-stratified flow, water waves like those in Figs. 4–7 move slowly down the flow channel [38–40]. We do not observe classical wavy-stratified flow in that the waves do not move continuously down the flow channel. Still the flow is analogous to wavy-stratified flow.

It is interesting to speculate why we see wavy flow, not slug flow. We believe that one key reason is that the Teflon treated GDL is much more hydrophobic than the graphite flow channels. If the all of the sides of the flow channel were equally wetting, one would expect to observe water on all sides on the flow channel. That would produce what is called annular flow at the flow rates of interest in fuel cells [38–40]. However, in a fuel cell the GDL surface is more hydrophobic than the graphite flow channel. The hydrophobic forces will push the water away from the hydrophobic surface producing wavy flow.

Once the wave forms on the bottom of the flow channel, it is pushed along via the viscous and shape forces produced by the air moving along the free surfaces of the wave (see Fig. 6). However, unlike in slug flow, the water does not move at the air velocity. In slug flow, the water goes all the way across the flow channel. In such a case, the only way for air to move is to push water along at the same velocity. However, in a fuel cell there is a gap between the water wave and the GDL as seen in Figs. 5 and 6. The air can flow through the gap, so the water velocity can be different than the air velocity.

In fact the water velocity is usually much lower than the air velocity in wavy-stratified flow. The viscous and shape forces from the moving air shown in Fig. 6 move the water wave along, but friction due to circulation of the fluid slows the water down. The

frictional forces on the water are much larger than the frictional forces on the air since water is much denser and more viscous than air. Consequently, the water waves move much more slowly than air.

Now consider what happens when the water wave hits a defect. The defect could be a small protrusion from the wall, a dust particle, or even a region of the wall that is especially hydrophobic or hydrophilic. In each case the wall defect will exert an extra force on the moving water wave. If the extra force is large enough, the wave will get stuck. Then the wave will need a larger force to get unstuck.

Water then accumulates in the stationary wave, as shown in Fig. 4 and the channel begins to fill up. The air velocity in the gap between the top of the water wave increases as the gap shrinks, which increases the viscous and shape forces. Eventually, the viscous and shape forces are large enough to push the water along.

In our experiments, we have never seen the flow channel filling entirely but channel filling could occur if the defect were large enough leading to an intermittent slug like flow.

The observation of slip and stick flow have some important implications to water management. First, stagnant water in the fuel cell would be unavailable in any system that sought to exploit water generated at the cathode to humidify other areas of the fuel cell. Second, water that has become stuck in the flow channel represents a danger to fuel cell operation in cold climates, as these are the locations most likely to freeze, and cause damage to the fuel cell. Third, the removal of water from the GDL surface happens due to lift forces, instead of being swept off the GDL surface by a passing slug, as predicted in slug flow. This correct mechanism of water removal must be accounted for in fuel cell modeling, if accurate models are to be attained. Another implication is the possibility of dead-zones, areas in the flow field channel with low velocity gas flow.

Of course, one does need to consider whether our results are artifacts of our experimental procedures. Our cell has especially deep flow channels which gives extra room for water to accumulate, as seen in neutron scattering experiments [7]. We also have graphite painted Teflon flow channels, rather than solid graphite. Still, the forces in our flow channel are the same as in the flow fields of a commercial cell. Therefore, it is likely that a similar mechanism of water transport will be seen.

Lastly, it is interesting to note, the initial transport of water through the porous cathode GDL was in agreement with the proposed mechanism for water transport through this hydrophobic medium [41]. The current mechanism states that water generated at the cathode slowly works its way into the hydrophobic pores of the cathode GDL via capillary action. The water works its way through the pores, until one 'branch' of water in one of the pores reaches the surface. Once an open pathway to the surface of the GDL is reached, it becomes the lowest energy pathway for the water pressure underneath the GDL to relieve itself and all water underneath the GDL follows this one pore to the surface. Therefore, one would expect large droplets to form on the GDL surface, instead of a uniform film. Our findings appear to support this theory.

A final observation was that electroosmosis appears to be the dominant mode of water transport through the Nafion® membrane, when the cell is run at 500 mA cm^{-2}. Diffusion and hydrophobic backpressure appear to dominate at 200 mA cm^{-2}. Clearly, there is a 'tipping point' where water will no longer be transported to the anode, which might lead to anode dehydration and additional overpotential due to increased membrane resistance due to reduced proton conductivity. Care will need to be taken to optimizing the fuel cell to insure adequate anode hydration while operating at high currents densities.

5. Conclusions

MRI was used to find the three-dimensional quantitative water distributions inside an operating fuel cell. Water generated at the cathode through the oxygen reduction reaction was found to first transport through the GDL and form a large drop on the GDL surface. Over time, the drops detached into the cathode flow field, where they assumed a wave-stratified pattern, not slug flow. The waves were mostly stationary, appearing to become 'stuck' on defects in the cathode flow field graphite coating. Although the waves were stationary most of the time, they would occasionally 'slip', and move down the flow field channel, always in the direction of gas flow, until becoming 'stuck' on another defect, or being exhausted from the cell entirely. Additionally, the electroosmotic forces came to dominate diffusional and hydrophobic backpressure forces as current density increases.

Acknowledgements

This research is funded by the Defense Advanced Research Projects Agency (DARPA) under grant DST 2007-0299513-000-1. Any opinions, findings and conclusions or recommendations expressed in this manuscript are those of the authors and do not necessarily reflect the views of the Defense Advanced Projects Research Agency or the US government.

References

[1] D. Cheddie, N. Munroe, Review and comparison of approaches to proton exchange membrane fuel cell modeling, J. Power Sources 147 (1/2) (2005) 72–84.
[2] L. Ma, et al., Review of the computational fluid dynamics modeling of fuel cells, J. Fuel Cell Sci. Technol. 2 (4) (2005) 246–257.
[3] C.Y. Wang, Fundamental models for fuel cell engineering, Chem. Rev. 104 (10) (2004) 4727–4766.
[4] P.W. Albers, et al., Inelastic neutron scattering investigation on the site occupation of atomic hydrogen on platinum particles of different size, J. Catal. 223 (1) (2004) 44–53.
[5] R.J. Bellows, et al., Neutron imaging technique for in situ measurement of water transport gradients within Nafion in polymer electrolyte fuel cells, J. Electrochem. Soc. 146 (3) (1999) 1099–1103.
[6] D. Kramer, et al., An on-line study of fuel cell behavior by thermal neutrons, Nuclear Instrum. Methods Phys. Res. Sec. A 542 (1–3) (2005) 52–60.
[7] D. Kramer, et al., In situ diagnostic of two-phase flow phenomena in polymer electrolyte fuel cells by neutron imaging. Part A. Experimental, data treatment, and quantification, Electrochim. Acta 50 (13) (2005) 2603–2614.
[8] N. Pekula, et al., Study of water distribution and transport in a polymer electrolyte fuel cell using neutron imaging, Nuclear Instrum. Methods Phys. Res. Sec. A 542 (1–3) (2005) 134–141.
[9] J.B. Zhang, et al., In situ diagnostic of two-phase flow phenomena in polymer electrolyte fuel cells by neutron imaging. Part B. Material variations, Electrochim. Acta 51 (13) (2006) 2715–2727.
[10] A.S. Arico, et al., An NMR and SAXS investigation of DMFC composite recast Nafion membranes containing ceramic fillers, J. Membr. Sci. 270 (1/2) (2006) 221–227.
[11] V.V. Binsu, et al., Studies on *N*-methylene phosphonic chitosan/poly(vinyl alcohol) composite proton-exchange membrane, React. Funct. Polym. 66 (12) (2006) 1619–1629.
[12] M.G. Compton, et al., Proton NMR relaxation study of the $CsHSO_4$ solid acid system, Solid State Commun. 136 (3) (2005) 138–141.
[13] D.S. Kim, H.B. Park, J.Y. Jang, Y.M. Lee, Synthesis of sulfonated poly(imidoaryl ether sulfone) membranes for polymer electrolyte membrane fuel cells, J. Polym. Sci. Part A: Polym. Chem. 43 (22) (2005) 5620–5631.
[14] H.A. Every, et al., An NMR study of methanol diffusion in polymer electrolyte fuel cell membranes, J. Membr. Sci. 250 (1/2) (2005) 183–188.
[15] K.W. Feindel, et al., In situ observations of water production and distribution in an operating H_2/O_2 PEM fuel cell assembly using ^1H NMR microscopy, J. Am. Chem. Soc. 126 (37) (2004) 11436–11437.
[16] I. Fischbach, et al., Solid state NMR spectroscopic investigations of model compounds for imidazole-based proton conductors, J. Phys. Chem. B 108 (48) (2004) 18500–18508.
[17] R. Guilard, et al., Synthesis and characterization of cofacial metallodiporphyrins involving cobalt and Lewis acid metals: new dinuclear multielectron redox catalysts of dioxygen reduction, J. Am. Chem. Soc. 117 (47) (1995) 11721–11729.

[18] J.D. Halla, et al., Meso-SiO_2-$C_{12}EO_{10}OH$-CF_3 SO_3H—a novel proton-conducting solid electrolyte, Adv. Funct. Mater. 13 (2) (2003) 133–138.
[19] J. Healy, et al., Aspects of the chemical degradation of PFSA ionomers used in PEM fuel cells, Fuel Cells 5 (2) (2005) 302–308.
[20] J.R.P. Jayakody, et al., NMR studies of mass transport in high-acid-content fuel cell membranes based on phosphoric acid and polybenzimidazole, J. Electrochem. Soc. 154 (2) (2007) B242–B246.
[21] T. Kazuhiro, T. Shohji, H. Shuichiro, Study of the effect of membrane thickness on the performance of polymer electrolyte fuel cells by water distribution in a membrane, Electrochem. Solid-State Lett. 8 (6) (2005) A281–A284.
[22] Y.J. Kim, et al., Synthesis of high molecular weight polybenzoxazoles in polyphosphoric acid and investigation of their hydrolytic stability under acidic conditions, High Perform. Polym. 17 (3) (2005) 377–401.
[23] C.N. Kostelansky, et al., Triarylphosphine-stabilized platinum nanoparticles in three-dimensional nanostructured films as active electrocatalysts, J. Phys. Chem. B 110 (43) (2006) 21487–21496.
[24] A. Noda, et al., Brønsted acid-base ionic liquids as proton-conducting nonaqueous electrolytes, J. Phys. Chem. B 107 (17) (2003) 4024–4033.
[25] X. Ren, et al., Methanol transport through nafion membranes electro-osmotic drag effects on potential step measurements, J. Electrochem. Soc. 147 (2) (2000) 466–474.
[26] T. Shohji, T. Kazuhiro, H. Shuichiro, Magnetic resonance imaging of the water distribution within a polymer electrolyte membrane in fuel cells, Electrochem. Solid-State Lett. 7 (9) (2004) A269–A272.
[27] L. Silvia, et al., Ormosil/sulfonated polyetheretherketone-based hybrid composite proton conducting membranes, J. Electrochem. Soc. 153 (6) (2006) A1226–A1231.
[28] T. Uma, A. Nakao, M. Nogami, Characterization and electrochemical properties of P_2O_5–ZrO_2–SiO_2 glasses as proton conducting electrolyte, Mater. Res. Bull. 41 (4) (2006) 817–824.
[29] K.W. Feindel, S.H. Bergens, R.E. Wasylishen, The use of H-1 NMR microscopy to study proton-exchange membrane fuel cells, Chem. Phys. Chem. 7 (1) (2006) 67–75.
[30] S. Ha, Z. Dunbar, R. Masel, Magnetic resonance imaging (MRI): a new tool for fuel cell research, Abstr. Pap. Am. Chem. Soc. 230 (2005) U1638–U1639.
[31] J.R.P. Jayakody, et al., NMR investigation of water and methanol transport in sulfonated polyareylenethioethersulfones for fuel cell applications, J. Power Sources 156 (2) (2006) 195–199.
[32] K. Teranishi, S. Tsushima, S. Hirai, Study of the effect of membrane thickness on the performance of polymer electrolyte fuel cells by water distribution in a membrane, Electrochem. Solid-State Lett. 8 (6) (2005) A281–A284.
[33] K. Teranishi, S. Tsushima, S. Hirai, Analysis of water transport in PEFCs by magnetic resonance imaging measurement, J. Electrochem. Soc. 153 (4) (2006) A664–A668.
[34] S. Tsushima, K. Teranishi, S. Hirai, Magnetic resonance imaging of the water distribution within a polymer electrolyte membrane in fuel cells, Electrochem. Solid-State Lett. 7 (9) (2004) A269–A272.
[35] S. Tsushima, et al., Water content distribution in a polymer electrolyte membrane for advanced fuel cell system with liquid water supply, Magn. Reson. Imaging 23 (2) (2005) 255–258.
[36] Z. Dunbar, R.I. Masel, Quantitative MRI study of water distribution during operation of a PEM fuel cell using Teflon(R) flow fields, J. Power Sources 171 (2) (2007) 678–687.
[37] M.S. Wilson, S. Gottesfeld, Thin-film catalyst layers for polymer electrolyte fuel cell electrodes, J. Appl. Electrochem. (1992) 22.
[38] M.K. Akbar, S.M. Ghiaasiaan, Stability of stratified gas–liquid flow in horizontal annular channels, Exp. Thermal Fluid Sci. 28 (1) (2003) 7–21.
[39] T.J. Hanratty, Hershman, Initiation of roll waves, AIChE J. 7 (1962) 488–497.
[40] G.B. Wallis, J.E. Dodson, The onset of slugging in horizontal stratified air-water flow, Int. J. Multiphase Flow 1 (1) (1973) 173–193.
[41] U. Pasaogullari, C.Y. Wang, Liquid water transport in gas diffusion layer of polymer electrolyte fuel cells, ECS (2004) A399–A406.